



Design and high efficient photoelectric-synergistic catalytic oxidation activity of 2D macroporous SnO_2 /1D TiO_2 nanotubes

Peiqiang Li^{a,b}, Guohua Zhao^{a,*}, Mingfang Li^a, Tongcheng Cao^a, Xiao Cui^a, Dongming Li^a

^a Department of Chemistry, Tongji University, 1239 Siping Road, 200092 Shanghai, China

^b Department of Chemistry, Shandong Agricultural University, 61 Daizong Road, 271018 Tai'an, China

ARTICLE INFO

Article history:

Received 21 June 2011

Received in revised form 31 October 2011

Accepted 3 November 2011

Available online 17 November 2011

Keywords:

One-dimensional titanium oxide nanotubes

Two-dimensional macroporous SnO_2

Photoelectric-synergistic catalyst

2,4-dichlorophenoxyacetic acid

ABSTRACT

A novel catalyst was constructed by assembling 1D TiO_2 nanotubes (TiO_2 NTs) photocatalyst and 2D macroporous SnO_2 electrocatalyst, which presents simultaneously the outstanding photocatalytic and electrocatalytic properties, and was applied to the photoelectric synergistic catalytic oxidation of biorefractory pollutants. Liquid crystal soft template was prepared by block copolymer self-assembly, and the macroporous SnO_2 membrane grew orderly on the TiO_2 NTs using the soft template by one-step assembly. The macroporous SnO_2 has the pore size distribution between 150 and 400 nm, small particle size (14.2 nm), and high loading amount (27.3 g m^{-2}). The band gap of the 2D macroporous SnO_2 / TiO_2 NTs is 2.93 eV. Compared with the general TiO_2 NTs and the SnO_2 / TiO_2 NTs, the 2D macroporous SnO_2 / TiO_2 NTs possess better optical absorption and photocatalytic properties, with a photoelectric conversion efficiency of 35.2% at 365 nm. Moreover, the hybrid anode presents smaller surface impedance and solution interface impedance, larger electrochemical surface absorption volume and lower electrochemical reaction activation energy. In the photoelectrocatalytic process, the 2D macroporous SnO_2 / TiO_2 NTs exhibited higher removal rate for 2,4-dichlorophenoxyacetic acid, the initial instantaneous current efficiency was 100%, and COD removal rate reached 90.1% within 3 h. The study showed that the intermediates was generated faster and removed quickly on the prepared catalyst.

© 2011 Elsevier B.V. All rights reserved.

1. Introduction

Photocatalytic (PC) and electrocatalytic (EC) oxidation are advanced oxidation technologies with different forms of energy conversion and distinguished catalytic characteristics used in the fields of environment, energy conversion/storage, and hydrolysis [1–4]. Therefore, the photoelectrocatalytic (PEC) technology that combines the advantages of the two technologies is significant in the theoretical and application prospects. The key is to explore novel PEC material that simultaneously presents excellent PC and EC ability [5,6].

In order for PC and EC to happen simultaneously at the same catalytic material surface, the catalytic species and the material properties are crucial. TiO_2 is an excellent photocatalyst [7,8], and the one-dimensional (1D) TiO_2 nanotubes (TiO_2 NTs) are more efficient than the other structure of TiO_2 , which can be easily prepared by electrochemical anodic oxidation [9]. With a highly ordered array arrangement, TiO_2 NTs present larger specific surface area and higher surface energy, so it has high PC efficiency [10,11]. However, TiO_2 is a semiconductor material with low conductivity and

poor EC performance, so TiO_2 NTs are suitable to work as an efficient photocatalyst, but not suitable to be an electrocatalyst. In the view of electrochemical oxidation, dimensionally stable anodes (DSA) are widely used in the chlor-alkali industry for its lower chlorine evolution potential. However, the oxygen evolution potential of DSA is also low. While the Sb doped SnO_2 coating anode has high oxygen evolution potential and superior EC performance [12], it will decrease the energy consumption of the hydrogen generation in the hydrolysis reaction and increase the current efficiency, so it is very suitable to use in the electrochemical oxidation synthesis, especially the electrochemical oxidation in aqueous media and environmental degradation of refractory pollutants [13,14]. However, SnO_2 is a semiconductor material, whose band gap is 3.88 eV [9], its PC efficiency is lower. So the key is to explore a novel integrated photoelectrocatalyst, which can realize that simultaneous PC and EC oxidation are synergistically generated at one catalytic material surface and in the same reaction process.

Herein, we think that it can sufficiently use the structure of the TiO_2 NTs. The ordered and vertical TiO_2 NTs arrays in situ grown on the surface of pure Ti sheet not only have larger specific surface area and higher surface energy, but also have higher adsorption capacity and more active sites. It can act as an ideal “container” or “supporter” to assemble the Sb doped SnO_2 electrocatalyst in the microstructure constructing a novel photoelectrocatalyst.

* Corresponding author. Tel.: +86 21 65988570x8244; fax: +86 21 65982287.
E-mail address: g.zhao@tongji.edu.cn (G. Zhao).

Assembling the Sb doped SnO_2 to the inside and surface of the TiO_2 NTs by sol–gel method, it can easily form the $\text{SnO}_2/\text{TiO}_2$ NTs catalyst [15,16]. The improved loading amount and dispersion of SnO_2 are helpful to strengthen the PC and EC performance of the prepared catalyst [17,18]. However, the preparation is complex and long-term, the loading was repeated several times [18]. Another is that a small quantity of antimony must be doped into SnO_2 to achieve excellent EC properties, although SnO_2 itself is light transmission agent, but Sb doped SnO_2 will decrease the light absorption [18]. So the object of the research is that the loading of the Sb doped SnO_2 will not affect the light absorption of TiO_2 NTs, and right way can be found to enhance the catalytic oxidation effect of photoelectric synergy.

Therefore, it was started with the construction of a novel photo-electrocatalyst by assembling the 2D macroporous SnO_2 to the 1D TiO_2 NTs, which is the first time report. The soft template, with block copolymer (styrene phenol polyoxyethylene ether, abbreviated as SPPE) self-assembly into ordered liquid crystal (LC) structure, is adopted in the preparation, it is the necessary condition to form the specific structure. Sb doped SnO_2 is assembled to the TiO_2 NTs using the LC soft template. The soft template is removed by calcination, 2D periodically ordered macroporous SnO_2 is successfully prepared. The preparation of the catalyst is one-step assembly, it is simple and time saving. The constructed way maybe have the following two advantages: one is that the 2D macroporous structure of SnO_2 makes the light permeate directly and increases the light absorption greatly. And it is reverse phase doping for SnO_2 and TiO_2 according to the energy band theory, which perhaps is suitable for the separation of photogenerated electrons and holes, and improves the photoconversion efficiency. The other is that the prepared method perhaps endows SnO_2 with small particle size, ordered arrangement and large loading amount, those will greatly improve the EC performance of the catalyst. Thus, in the experiment, we studied the fabrication of the catalyst, and the catalyst's photoelectric synergistic catalytic property. Furthermore, the properties of the catalysts were investigated by applying to the degradation of 2,4-dichlorophenoxyacetic acid (2,4-D) [19,20], 2,4-D is a phenoxy carboxylic acid herbicide, which is widely used in crop weeding and lawn maintenance in large amount and long time. It has mutagenicity and teratogenicity, and it is difficult to be biochemical degraded, whose chlorine-containing metabolic intermediates are of high toxicity [21]. Therefore, 2,4-D pollution has become an environmental problem needed to be resolved urgently [22,23]. In the further study, it elaborated the high efficiency and oxidation mechanism of the 2D macroporous $\text{SnO}_2/\text{TiO}_2$ NTs from the generation and further oxidation of the intermediate. This study provides a new idea for exploring the catalyst with high photoelectric synergistic performance.

2. Experimental

2.1. Preparation of 2D macroporous $\text{SnO}_2/\text{TiO}_2$ NTs

TiO_2 NTs were prepared by the electrochemical anodic oxidation method according to the literature [18]. The preparation of precursor is as follows. 6.0 g of SPPE (number average molecular weight $\bar{M}_n = 1622$, relative molecular mass distribution width $D = 1.10$) is dissolved in 3.0 g water, forming solution A. 3.0 g $\text{SnCl}_2 \cdot 2\text{H}_2\text{O}$ and 0.15 g SbCl_3 are dissolved in 3.0 g 18 wt% hydrochloric acid, forming solution B. Solution C is formed by mixing A and B solutions. TiO_2 NTs are put into the buffer bottle and solution C is added after vacuuming to 6×10^{-2} Pa. The electrode is immersed in solution C for 5 min, aged to membrane at 40°C for 24 h, dried at 100°C for 30 min, dried at 300°C for 30 min, and pyrolyzed at 500°C for 1 h, and the 2D macroporous $\text{SnO}_2/\text{TiO}_2$ NTs is prepared (Scheme 1).

The preparation of $\text{SnO}_2/\text{TiO}_2$ NTs refers to the literature [24], which is prepared by sol–gel method and the dip-coating is repeated ten times.

2.2. Characterization of the surface structure and physicochemical properties

The morphology of catalyst is characterized by the field emission environmental scanning electron microscopy (FESEM, Model Quanta 200 FEG, manufacturer FEI). The crystal structure of catalyst is characterized by the X-ray diffraction analysis (XRD, Model D/max2550VB3+/PC, manufacturer Rigaku). The optical absorption characteristics are determined by UV–visible diffuse reflectance spectroscopy (UV–vis DRS, Model BWS002, manufacturer BWtek). The sample's surface area is measured using BET analysis system (Autosorb-iQ, manufacturer Quantachrome).

Photoelectrochemical properties are measured in the three-electrode system of CHI660C electrochemical workstation. $\text{SnO}_2/\text{TiO}_2$ NTs, TiO_2 NTs and 2D macroporous $\text{SnO}_2/\text{TiO}_2$ NTs work as the anode, platinum plate as the counter electrode, and saturated calomel electrode as the reference electrode. Cyclic voltammetry (CV) is used to test the catalyst's electrochemical properties, and the sweep speed is 50 mV s^{-1} . Electrochemical impedance spectroscopy (EIS) is used to determine the conductivity of the catalysts, with the frequency range from 1×10^5 to 1×10^{-3} Hz and amplitude 5 mV. The electrolyte is 0.05 M $[\text{Fe}(\text{CN})_6]^{3-}/[\text{Fe}(\text{CN})_6]^{4-}$ solution.

The activation energy (E_a) of the catalyst is measured according to the anodic polarization curves of electrodes at different temperature in the 0.1 M H_2SO_4 . The E_a value is determined in accordance with the law of Arrhenius [25]:

$$\lg i = \frac{E_a}{2.303RT} + \text{Const} \quad (1)$$

It is a linear relation between $\lg i$ and $1/T$, and E_a of the catalyst can be determined by the slope of the straight line.

Photocurrent density is measured in 1 M KOH. 15 W UV lamp (center wavelength 254 nm, light intensity 9 mW cm^{-2}) and 300 W UV lamp (center wavelength 365 nm, light intensity 3 mW cm^{-2}) are used as the UV light source, and 500 W xenon lamp (center wavelength 420 nm, light intensity 1.8 mW cm^{-2}) is used as the visible light source. The photoelectric conversion efficiency is calculated according to the literature [26].

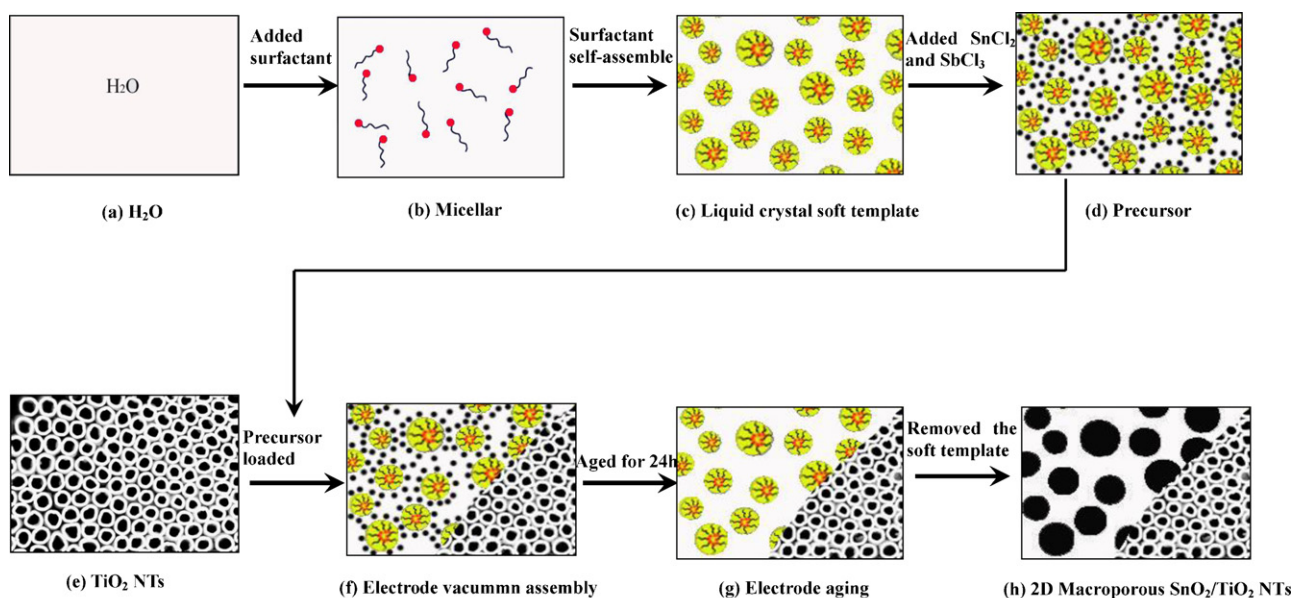
2.3. PEC degradation experiment

PEC degradation experiment is carried out in a round reaction pool, in which water is recycled in order to maintain the reaction temperature at 25°C . The 2D macroporous $\text{SnO}_2/\text{TiO}_2$ NTs, $\text{SnO}_2/\text{TiO}_2$ NTs and TiO_2 NTs work as the anode, titanium as cathode, electrode area is 3 cm^2 , electrode gap is 1.0 cm, and the current density is 10 mA cm^{-2} . 300 W UV lamp is the light source. 0.1 M Na_2SO_4 containing 100 mg L^{-1} 2,4-D is used as the simulated wastewater, and the solution volume is 100 mL.

Concentrations of 2,4-D and the intermediates are tested by HPLC (Varian 3900 HPLC). The samples are detected and quantified by AQ-C18 ($4.6 \times 100 \text{ mm}$, $5 \mu\text{m}$) and selected UV detector at $\lambda = 230 \text{ nm}$. 40:60 (v/v) methanol/phosphate buffer (pH 2.3) is employed as the mobile phase at the flow rate of 0.8 mL min^{-1} .

Instantaneous current efficiency (ICE) can be expressed as follows [27],

$$\text{ICE} = \frac{FV}{8000I} \frac{d(\text{COD})}{dt} \quad (2)$$



Note: (left of f–h) loaded precursor part, (right of f–h) unloaded part.

Scheme 1. Schematic illustration for the 2D macroporous $\text{SnO}_2/\text{TiO}_2$ NTs growth.

$d(\text{COD})$ is the volume change of COD in time dt , mg L^{-1} ; t is the electrolysis time, s; I is the current intensity, A; V is the electrolyte volume. COD is determined by dichromate method.

3. Results and discussion

3.1. Preparation and characterization of the novel catalyst

In the experiment, surfactant solution first form the micelles (Scheme 1b), then micelles spontaneously form the advanced homogeneous lyotropic LC with columnar structure when the macromolecule block copolymer surfactant of SPPE reaches certain concentration (Scheme 1c). The LC is a special orderly arranged structure, with high viscosity and transparent appearance. With LC as the template, it has strong interaction between the tin–antimony ions and the LC molecules (Scheme 1d), then the controlled growth of SnO_2 on the TiO_2 NTs (Scheme 1e) is realized (Scheme 1f, g, h).

Fig. 1a and b shows the top view of macroporous $\text{SnO}_2/\text{TiO}_2$ NTs with low and high magnification, respectively. It can be seen from the scanning electron microscopy (SEM) that SnO_2 grows to an orderly 2D periodic nanohole membrane. The nanoholes are close to each other, with circular orifices and diameters from 150 to 400 nm, which are formed with the removal of columnar structured LC template. The hole walls with upper and lower permeation are linked to each other, and TiO_2 NTs can be seen through the nanohole (Fig. 1c). Compared with the particle membrane (Fig. S1 in supporting information) of the $\text{SnO}_2/\text{TiO}_2$ NTs, the macroporous SnO_2 film is very smooth. The reason is that the interaction between the surfactant and inorganic molecules (mainly electrostatic forces and hydrogen bonding) is induced, when the surfactant solution and the tin–antimony solution are mixed (Scheme 1d). The inorganic molecules will grow along the alignment direction of LC template and form an ordered membrane structure [28]. The smooth surface of the macroporous SnO_2 also indicates that the particles are small and uniformly distributed. The crystal structure of the electrode surface is studied by X-ray diffraction analysis (XRD) (Fig. 2), it can be seen that the diffraction peak of SnO_2 was clearly enhanced. The SnO_2 particle size is calculated by the Scherrer formula ($D = k\lambda / \beta \cos \theta$) [12], which is 14.2 nm on

the surface of the 2D macroporous $\text{SnO}_2/\text{TiO}_2$ NTs and is small for metal oxide particles. The SnO_2 particle size of SnO_2/Ti prepared by traditional brushing method is about 0.1–1 μm , and that prepared on the TiO_2 NTs by sol–gel in virtue of silicone surfactant is 22.9 nm [18]. After samples had been vacuum-dried at 200 $^\circ\text{C}$ overnight, nitrogen adsorption–desorption isotherms are measured at 77 K on a Autosorb-iQ (Fig. S2 in supporting information). The surface area of the 2D macroporous $\text{SnO}_2/\text{TiO}_2$ NTs and SnO_2/Ti is 642 and 351 $\text{m}^2 \text{g}^{-1}$, respectively (Table 1). Therefore, SnO_2 prepared by LC soft template not only exhibits 2D periodic porous structure, but also has smaller particle size, surface area and higher dispersion. The high degree of dispersion and surface area may improve the PEC performance. The assembly of SnO_2 by LC soft template has another important advantage, high loading amount, since its electrochemical activity is closely related to the loading amount of the electrocatalyst. In order to obtain good electrochemical properties, it needs to load many times in the traditional sol–gel method, so that the procedure is long and complex. Without anodizing pretreatment for the Ti base, after loading ten times directly in the tin–antimony sol, the SnO_2 loading is 8.2 g m^{-2} , average 0.82 g m^{-2} each time. With the advantage of the space of TiO_2 NTs, the SnO_2 loading can be increased to 21.4 g m^{-2} after loading ten times, average 2.14 g m^{-2} each time. Using LC soft template, the SnO_2 loading is improved to 27.3 g m^{-2} one-time assembly, which is 33 times and 13 times that by the other two methods, respectively. Consequently, the electrocatalyst is assembled by LC soft template simply with time saving. The reason is that once the surfactant is

Table 1
Photoelectrochemical parameters of the three catalysts.

	TiO_2 NTs	$\text{SnO}_2/\text{TiO}_2$ NTs	2D macroporous $\text{SnO}_2/\text{TiO}_2$ NTs
E_g (eV)	3.22	2.93	2.93
η_{max} (%)	7.1	28.6	35.2
R_p (Ω)	31196	590	473
R_s (Ω)	107.3	21.5	18.2
C (mF)	0.058	0.382	1.890
G (mol cm^{-2})	–	3.91×10^{-10}	2.07×10^{-9}
E_a (J mol^{-1})	38.0	34.7	27.3
A_{BET} ($\text{m}^2 \text{g}^{-1}$)	–	351	642

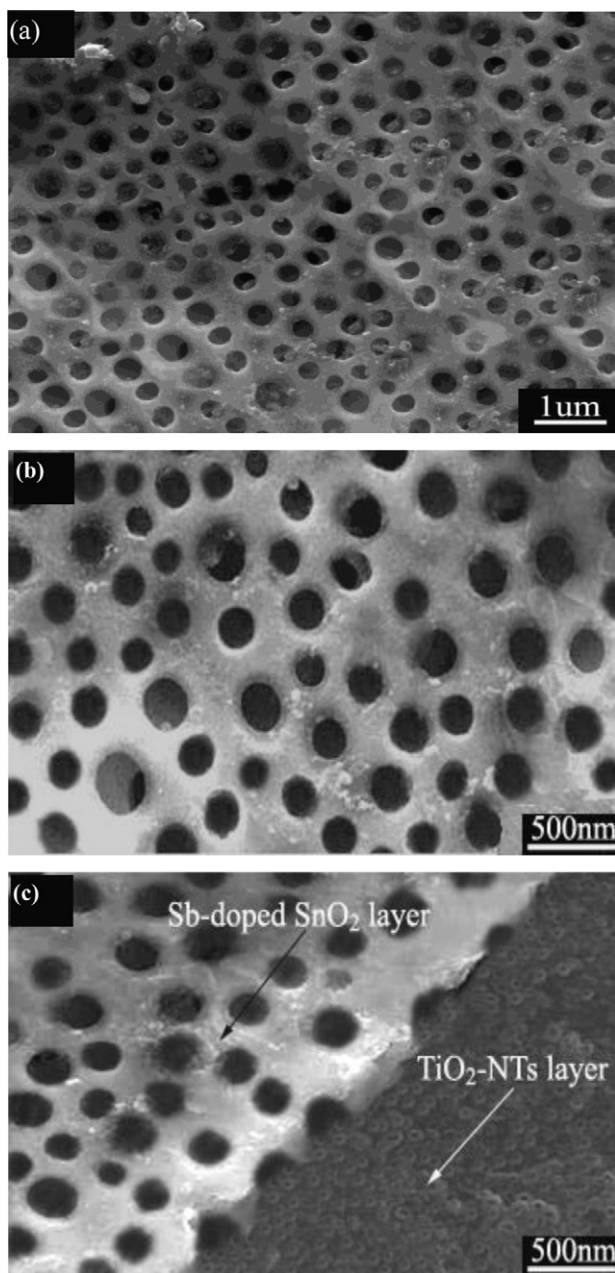


Fig. 1. (a) SEM top view of the 2D macroporous $\text{SnO}_2/\text{TiO}_2$ NTs with low magnification. (b) SEM top view of the 2D macroporous $\text{SnO}_2/\text{TiO}_2$ NTs with high magnification. (c) SEM side view of the 2D macroporous $\text{SnO}_2/\text{TiO}_2$ NTs.

aggregated into the LC zone, the system becomes viscous because of the strong interaction among LC internal molecules, so a high loading amount is obtained one time.

3.2. PC performance

Catalyst's optical absorption property is an important prerequisite for photocatalysis. It is generally believed that the red shift of absorption band edge and increase in absorption intensity can improve the PC activity. Fig. 3a shows the UV–vis diffuse reflectance spectroscopy (UV–vis DRS) of the three catalysts, in which the absorption band edge of TiO_2 NTs is 385 nm and its ultraviolet absorption band is continuous in the range of 250–300 nm, but the absorptive capacity of TiO_2 NTs for the long-wavelength ultraviolet declines sharply in the range of 300–370 nm. The

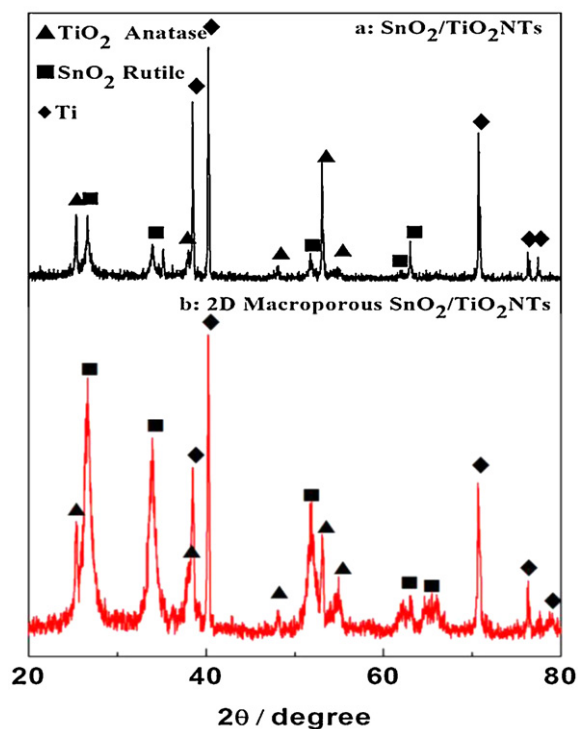


Fig. 2. XRD of (a): $\text{SnO}_2/\text{TiO}_2$ NTs and (b): 2D macroporous $\text{SnO}_2/\text{TiO}_2$ NTs.

absorption band of the two $\text{SnO}_2/\text{TiO}_2$ NTs catalysts exhibits distinct red shift with the SnO_2 assembled into the TiO_2 NTs. Whether the macroporous structure or the coating structure that evenly spreads into or outside the TiO_2 NTs, the absorption band edge is 424 nm, and the ultraviolet absorption band shifts to 300–370 nm. Compared with the TiO_2 NTs, the two $\text{SnO}_2/\text{TiO}_2$ NTs have better absorptive intensity in the long-wavelength range above 370 nm. The band gap (E_g) of TiO_2 NTs is 3.22 eV according to $E_g = 1240/\lambda$. The E_g of both $\text{SnO}_2/\text{TiO}_2$ NTs is 2.93 eV. Since the E_g of the semiconductor is significantly narrower, it is easier to be excited, which can be explained by the band gap matching between the SnO_2 and TiO_2 NTs (Fig. 3b). It is reverse doping between SnO_2 and TiO_2 , for TiO_2 has a lower E_g (3.22 eV) than SnO_2 (3.88 eV). When it is irradiated, TiO_2 is excited as a sensitizer to generate electron and hole [29]. As the valence band and conduction band of TiO_2 are lower than those of SnO_2 , the excited electron transits to the SnO_2 layer, which changes the bottom of the conduction band of TiO_2 , reducing its E_g . The holes spread correspondingly to the TiO_2 layer. The more holes reach the surface of TiO_2 generating oxidation reaction, the more electrons will be delivered to SnO_2 . SnO_2 is equivalent to an excellent electric conductor, which transfers electrons to the surface, inhibits the recombination of photo-generated electrons and holes, and improves the photoelectric separation efficiency. It helps to improve the PC performance. Compared with the ultraviolet absorption (250–370 nm) of TiO_2 NTs, that of the $\text{SnO}_2/\text{TiO}_2$ NTs declines with Sb doped, the Sb doping can be confirmed by the XPS test (Fig. S3 in the supporting information), the Sb doping can improve the electrical conductivity of the SnO_2 [30], but it hindered the light absorption in some extent. It can overcome the defect when the coating SnO_2 membrane is constructed to 2D macroporous structure. The 2D macroporous $\text{SnO}_2/\text{TiO}_2$ NTs displays the best light absorption characteristics in the whole region of light wavelength. This is contributed to the special constructed microstructure. The vertical thickness of the SnO_2 coating is about 100 nm, and the horizontal direction has 2D nanoscale pore structure (Fig. 1b), which has good light transparent effect, so that the

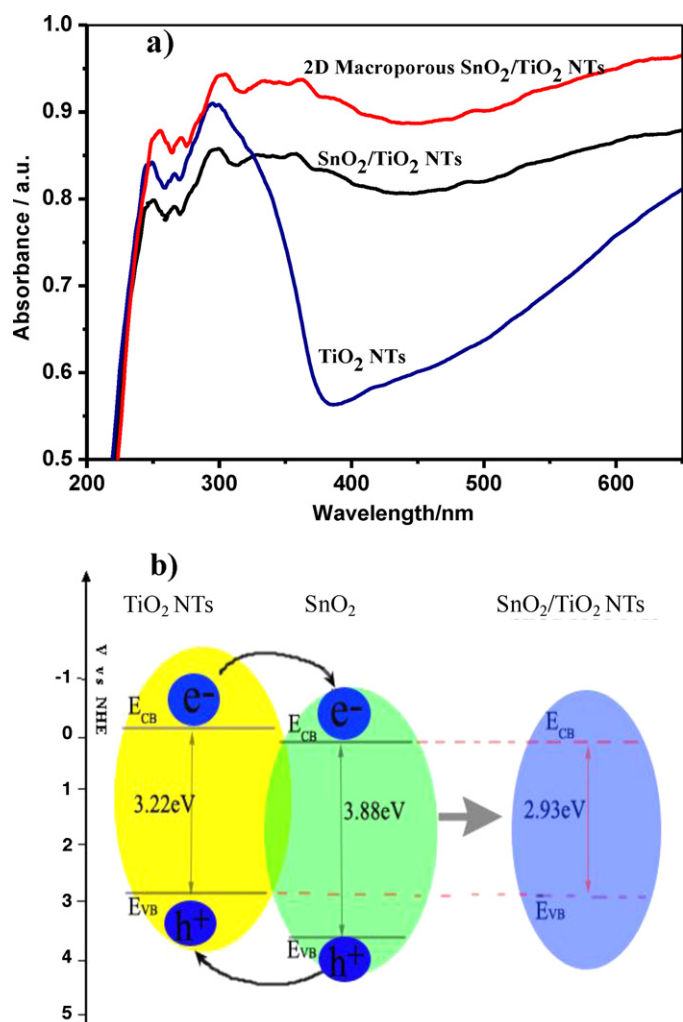


Fig. 3. (a) UV-vis DRS of 2D macroporous $\text{SnO}_2/\text{TiO}_2$ NTs, $\text{SnO}_2/\text{TiO}_2$ NTs and TiO_2 NTs. (b) E_g of $\text{SnO}_2/\text{TiO}_2$ NTs.

light can directly reach the surface of SnO_2 and TiO_2 to enhance the light absorption.

The photoelectric conversion efficiency (η) of the three catalysts is also compared. Fig. 4 shows that the current density changes with potential. At 365 nm, the current density of the macroporous $\text{SnO}_2/\text{TiO}_2$ NTs is the largest, and that of TiO_2 NTs is the smallest. The calculated maximum η of TiO_2 NTs, $\text{SnO}_2/\text{TiO}_2$ NTs and macroporous $\text{SnO}_2/\text{TiO}_2$ NTs at 365 nm is 7.1, 28.6 and 35.2%, respectively. This shows that the η of TiO_2 NTs is greatly improved after hybrid with Sb doped SnO_2 . Moreover, the microstructure of SnO_2 will affect the η . High η of 35.2% is obtained on the macroporous $\text{SnO}_2/\text{TiO}_2$ NTs, while it is only 15–30% on the common modified or doped TiO_2 [31,32]. The results also show that the change of photocurrent density is similar at 254 and 420 nm for the same surface structured material (Fig. 4).

3.3. EC performance

The electrochemical parameters are presented in Table 1. With the poor conductivity, the resistance of the catalyst itself (R_p) and the resistance between the catalyst and electrolyte (R_s) of TiO_2 NTs is large, 31196 and 107 Ω , respectively (Fig. S4 in supporting information), so that the TiO_2 NTs is unsuitable for electrochemical reactions. The conductivity of the two $\text{SnO}_2/\text{TiO}_2$ NTs is greatly improved: R_p is 400–600 Ω , and R_s is about 20 Ω after the

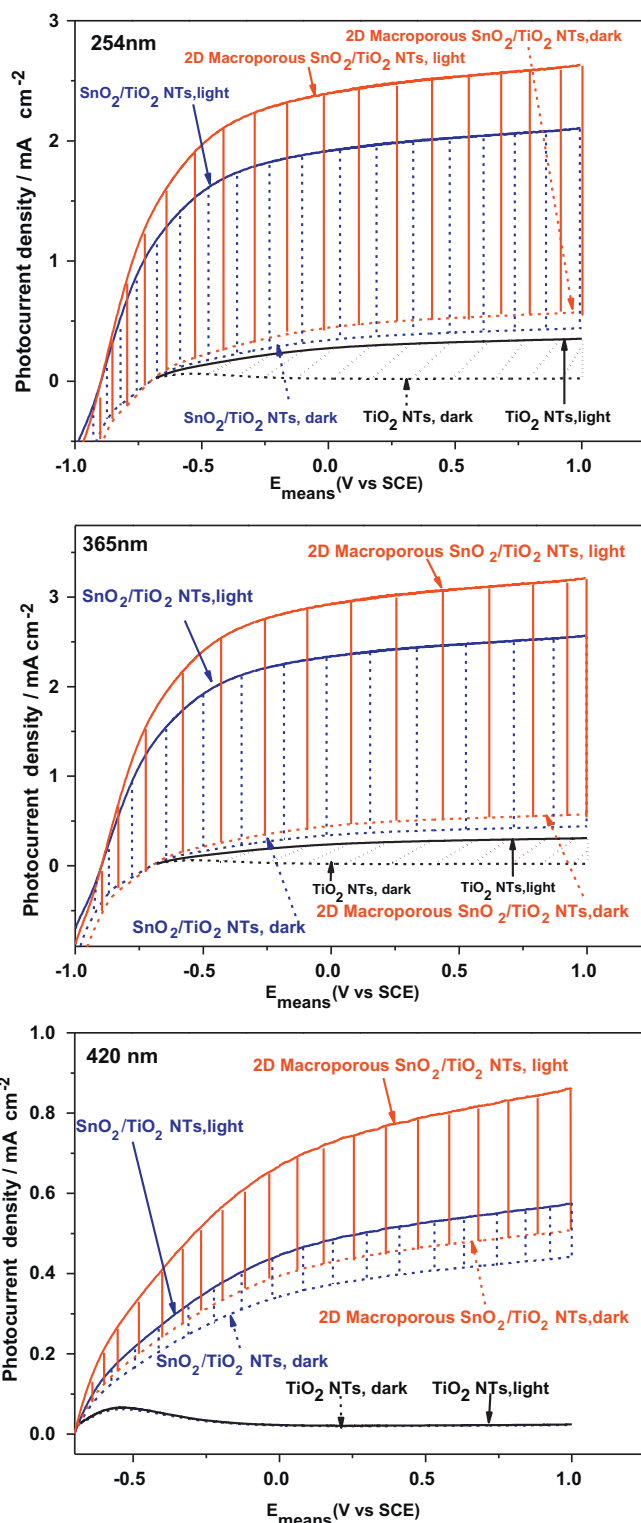


Fig. 4. Photocurrent density vs. bias potential (vs. SCE) at 254 nm, 365 nm and 420 nm.

modification of SnO_2 on TiO_2 NTs. Compared with $\text{SnO}_2/\text{TiO}_2$ NTs, 2D macroporous $\text{SnO}_2/\text{TiO}_2$ NTs has better conductivity with smaller R_p and R_s . The loading amount of SnO_2 per unit area on the 2D macroporous $\text{SnO}_2/\text{TiO}_2$ NTs is significantly higher than that of the $\text{SnO}_2/\text{TiO}_2$ NTs, and the small particle size of SnO_2 will improve the electrochemical properties of catalyst and lead to lower R_p . On the other hand, it may be related to the surface

hydrophilic property. The contact angle between water and $\text{SnO}_2/\text{TiO}_2$ NTs is 20° , while water can well spread on the 2D macroporous $\text{SnO}_2/\text{TiO}_2$ NTs surface, the contact angle of which is lower than 10° (Fig. S5 in supporting information). The macroporous SnO_2 makes the surface more hydrophilic, declining the value of R_s . The surface characteristics of the 2D macroporous $\text{SnO}_2/\text{TiO}_2$ NTs also affect another important catalyst property, the double-layer capacitance. Higher double-layer capacitance leads to charge transfer in a shorter time on the catalyst surface. Compared with the $\text{SnO}_2/\text{TiO}_2$ NTs, the double-layer capacitance of 2D macroporous $\text{SnO}_2/\text{TiO}_2$ NTs is increased almost an order of magnitude (Table 1), which indicates that the material may have higher adsorption and desorption rate in oxidation reaction.

The surface adsorption volume (G) of 2,4-D was measured on the two $\text{SnO}_2/\text{TiO}_2$ NTs catalysts by single potential step method (Fig. S6 in supporting information). The more pollutant G on the catalyst surface, the more reaction volume of electrochemical oxidation will perhaps occur. Under the same conditions, G is 3.91×10^{-10} and $2.07 \times 10^{-9} \text{ mol cm}^{-2}$ on the $\text{SnO}_2/\text{TiO}_2$ NTs and 2D macroporous $\text{SnO}_2/\text{TiO}_2$ NTs, respectively (Table 1), the latter being 5.3 times the former. Therefore, the microstructure of macroporous SnO_2 is helpful to improve the oxidation probability of the pollutants.

The special microstructure and surface chemical property of the macroporous SnO_2 may result in higher EC characteristics. E_a is obtained by measuring the anodic polarization curves. E_a of the 2D macroporous $\text{SnO}_2/\text{TiO}_2$ NTs, $\text{SnO}_2/\text{TiO}_2$ NTs and TiO_2 NTs is 27.3, 34.7 and 38.0 J mol^{-1} (Table 1), respectively. The 2D macroporous $\text{SnO}_2/\text{TiO}_2$ NTs needs the minimum E_a for reaction, while the TiO_2 NTs needs the highest. It shows that the 2D macroporous $\text{SnO}_2/\text{TiO}_2$ NTs has excellent EC performance. The results further confirm the conclusion by comparing the cyclic voltammetry curves of the three catalysts (Fig. S7 in supporting information).

3.4. Photoelectric synergistic degradation for 2,4-D

The properties of the catalysts were investigated by applying to the degradation of 2,4-D. The photoelectrocatalytic oxidation ability of the two $\text{SnO}_2/\text{TiO}_2$ NTs catalysts was compared emphatically. The removal rates of 2,4-D, chemical oxygen demand (COD) and the instantaneous current efficiency (ICE) were investigated in three processes, i.e., PC oxidation only, EC oxidation only and the integrated PEC oxidation.

Fig. 5a shows the 2,4-D removal rate in the three processes. The corresponding removal rate in the PC reaction is 57.3, 51.7 and 31.0% on the 2D macroporous $\text{SnO}_2/\text{TiO}_2$ NTs, $\text{SnO}_2/\text{TiO}_2$ NTs and TiO_2 NTs, respectively. In the EC process, the removal rate of the two $\text{SnO}_2/\text{TiO}_2$ NTs reaches 85.9 and 72.6%, respectively. In the PEC process, 2,4-D is completely transformed on the 2D macroporous $\text{SnO}_2/\text{TiO}_2$ NTs in 1.5 h, while it needs 2.5 h on the $\text{SnO}_2/\text{TiO}_2$ NTs and longer time on the TiO_2 NTs. Dynamic data show that the 2,4-D conversion fits the first order reaction because it shows a good linear relationship between $\ln C_{2,4-D}$ and t (Fig. 5b). The apparent rate constant of 2,4-D conversion on the 2D macroporous $\text{SnO}_2/\text{TiO}_2$ NTs, $\text{SnO}_2/\text{TiO}_2$ NTs and TiO_2 NTs is calculated, which is 0.31, 0.24 and 0.12 s^{-1} , respectively, in the PC reaction. For 2D macroporous $\text{SnO}_2/\text{TiO}_2$ NTs and $\text{SnO}_2/\text{TiO}_2$ NTs, the apparent rate constant is 0.63 and 0.44 s^{-1} in the EC reaction, and 2.06 and 1.24 s^{-1} in the PEC reaction, respectively. Therefore, the 2D macroporous $\text{SnO}_2/\text{TiO}_2$ NTs is more effective to remove 2,4-D, it has the best PEC properties and oxidation ability.

COD removal is shown in Fig. 6a. The removal rate of COD on the 2D macroporous $\text{SnO}_2/\text{TiO}_2$ NTs is higher than that on the $\text{SnO}_2/\text{TiO}_2$ NTs and TiO_2 NTs in the three reaction processes. 2,4-D contains conjugated aromatic structure, which is stable and difficulty open for epoxidation. COD removal rate on TiO_2 NTs is 20.5%

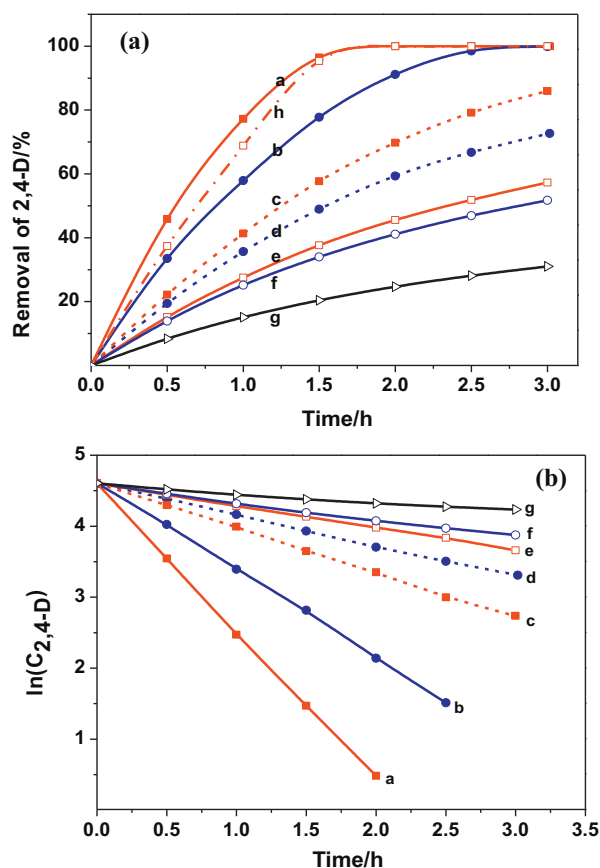


Fig. 5. (a) Removal rate of 2,4-D vs. time. (b) The relationship between $\ln C_{2,4-D}$ and time. Note: Line a: 2D macroporous $\text{SnO}_2/\text{TiO}_2$ NTs, PEC. Line b: $\text{SnO}_2/\text{TiO}_2$ NTs, PEC. Line c: 2D macroporous $\text{SnO}_2/\text{TiO}_2$ NTs, EC. Line d: $\text{SnO}_2/\text{TiO}_2$ NTs, EC. Line e: 2D macroporous $\text{SnO}_2/\text{TiO}_2$ NTs, PC. Line f: $\text{SnO}_2/\text{TiO}_2$ NTs, PC. Line g: TiO_2 NTs, PC. Line h: the addition of PC and EC on the 2D macroporous $\text{SnO}_2/\text{TiO}_2$ NTs.

in the PC process, while it is improved to 32.9% on the 2D macroporous $\text{SnO}_2/\text{TiO}_2$ NTs. COD removal on the $\text{SnO}_2/\text{TiO}_2$ NTs is 40.5% in the EC process, while it is improved to 47.7% on the 2D macroporous $\text{SnO}_2/\text{TiO}_2$ NTs. The COD removal rate on the 2D macroporous $\text{SnO}_2/\text{TiO}_2$ NTs is 90.1% in the PEC process, higher than 62.5% on the $\text{SnO}_2/\text{TiO}_2$ NTs. It indicates that the 2D macroporous $\text{SnO}_2/\text{TiO}_2$ NTs not only has good PC and EC effects, but also results in significant synergistic effect in the PEC process.

ICE of catalysts under different catalytic conditions was also tested (Fig. 6b). The traditional SnO_2/Ti coated electrode (Ti-based anode without electrochemical anodic oxidation and without TiO_2 NTs) has lower ICE in the EC reaction, only 18.2%. It is improved to 28.6% on the $\text{SnO}_2/\text{TiO}_2$ NTs, and to 37.9% on the 2D macroporous $\text{SnO}_2/\text{TiO}_2$ NTs. The result may be due to the different EC activity in different SnO_2 structures. The 2D macroporous $\text{SnO}_2/\text{TiO}_2$ NTs has a higher loading amount of electrocatalyst, smaller size of SnO_2 and lower E_a , so that its oxidation efficiency for 2,4-D is higher. In the PEC process, the initial ICE of the 2D macroporous $\text{SnO}_2/\text{TiO}_2$ NTs reaches 100%, which is obviously improved, while the ICE of the $\text{SnO}_2/\text{TiO}_2$ NTs is improved to some extent.

A synergistic effect of PC and EC processes occurs on the 2D macroporous $\text{SnO}_2/\text{TiO}_2$ NTs. Compared with the simple addition of the 2,4-D removal in the separate PC and EC process, the actual PEC oxidation efficiency for 2,4-D is much higher (Fig. 5a, line a, h). Similarly, the actual COD removal on the 2D macroporous $\text{SnO}_2/\text{TiO}_2$ NTs is higher than the simple addition of COD removal in the separate PC and EC process (Fig. 6a, line a, h). Those results indicate that the synergistic function of PC and EC process is indeed generated on this catalyst surface.

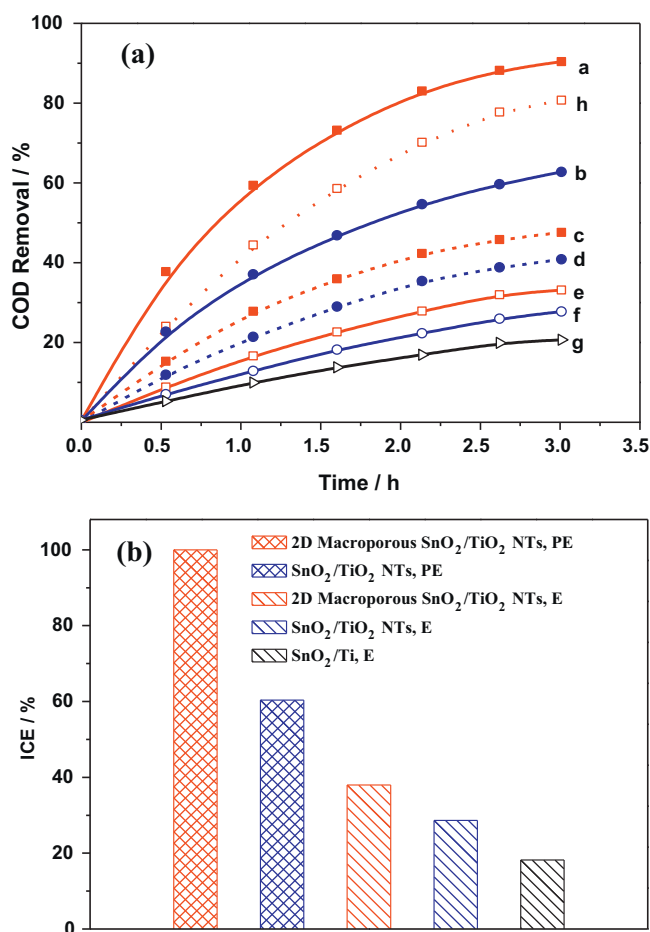


Fig. 6. (a) Removal rate of COD vs. time. (b) The ICE of the initial reaction on the 2D macroporous SnO₂/TiO₂ NTs, SnO₂/TiO₂ NTs and SnO₂/Ti catalysts. Note: Line a: 2D macroporous SnO₂/TiO₂ NTs, PEC. Line b: SnO₂/TiO₂ NTs, PEC. Line c: 2D macroporous SnO₂/TiO₂ NTs, EC. Line d: SnO₂/TiO₂ NTs, EC. Line e: 2D macroporous SnO₂/TiO₂ NTs, PC. Line f: SnO₂/TiO₂ NTs, PC. Line g: TiO₂ NTs, PC. Line h: the addition of PC and EC on the 2D macroporous SnO₂/TiO₂ NTs.

2D macroporous SnO₂/TiO₂ NTs simultaneously presents PC and EC characteristics. The light irradiation makes the active sites on the electrode surface fully expose, which overcomes the shortcoming that the active sites are easy to be inactive without the light irradiation and improves the electrochemical current efficiency. At the same time, the good conductivity of the electrode not only promotes the separation of the photo-generated electron-hole and increases the photoelectric efficiency, but also makes the PC oxidation less blocked because the species can be easily eliminated by EC oxidation.

3.5. Generation and further oxidation of the intermediates

The intermediates on the two SnO₂/TiO₂ NTs catalysts were investigated, it is the same on the two catalysts. The main benzene

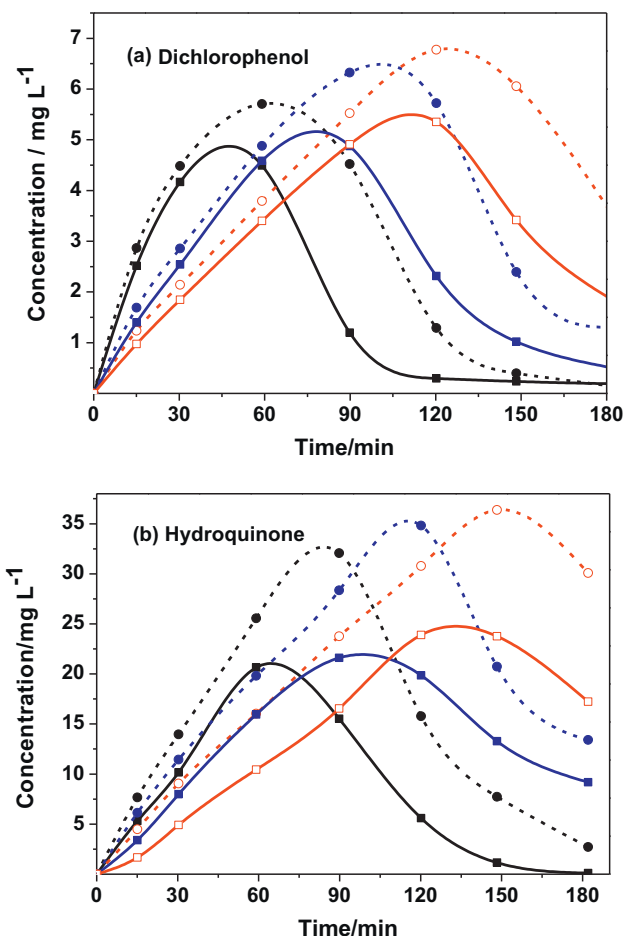
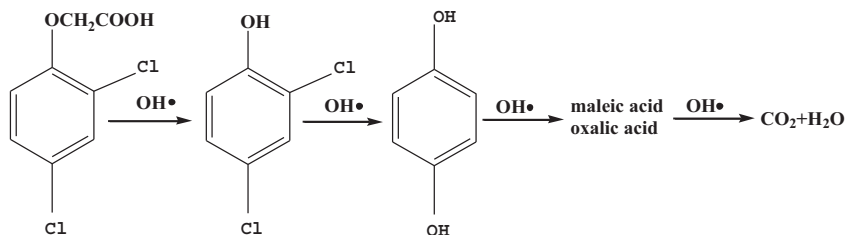


Fig. 7. Generation and further degradation of benzene ring-type intermediates. Note: Solid lines and dotted lines represent the 2D macroporous SnO₂/TiO₂ NTs and SnO₂/TiO₂ NTs, respectively. Black, blue and red line is the PEC, EC and PC process respectively. (For interpretation of the references to color in this figure legend, the reader is referred to the web version of the article.)

ring-type intermediates detected were 2,4-dichlorophenol and hydroquinone (Fig. 7a and b). The main acid intermediates were maleic acid and oxalic acid (Fig. 8a and b). And the following is different. Compared with the SnO₂/TiO₂ NTs, the maximum concentration of the benzene ring-type and the carboxylic acid intermediates are higher in the PC, EC and PEC process on the 2D macroporous SnO₂/TiO₂ NTs, and it needs shorter time to reach the maximum concentration and to be removed further. This is contributed to the small particle size and the 2D macroporous structure of SnO₂, which makes the 2D macroporous SnO₂/TiO₂ NTs has better PC, EC and PEC performance than the SnO₂/TiO₂ NTs. The conclusion is well accordance with the previous photoelectrochemical properties of the two catalysts.

On the 2D macroporous SnO₂/TiO₂ NTs, the concentration of hydroquinone, 2,4-dichlorophenol, maleic acid and oxalic acid is



Scheme 2. The possible degradation pathway of 2,4-D.

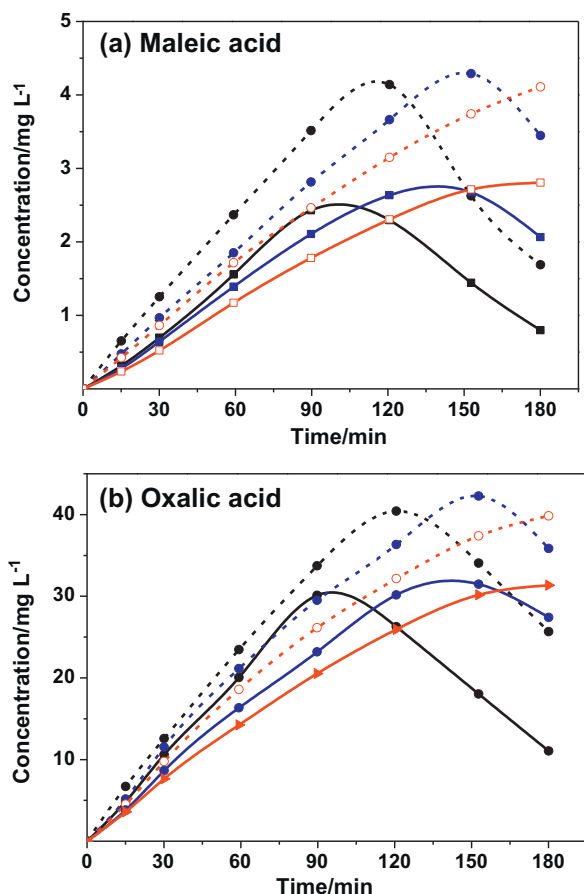


Fig. 8. Generation and further degradation of the carboxylic acid intermediates. Note: solid lines and dotted lines represent the 2D macroporous $\text{SnO}_2/\text{TiO}_2$ NTs and $\text{SnO}_2/\text{TiO}_2$ NTs, respectively. Black, blue and red line is the PEC, EC and PC process respectively. (For interpretation of the references to color in this figure legend, the reader is referred to the web version of the article.)

20.90, 4.87, 2.61 and 30.90 mg L^{-1} , respectively, in the EC process. They are 24.10, 5.40, 2.79 and 31.60 mg L^{-1} in the PC process, and 18.00, 4.27, 2.31 and 27.90 mg L^{-1} in the PEC process. The maximum concentration of intermediate in the PEC process is lower than those in the PC and EC process, and it needs shorter time to reach the maximum concentration and to be removed further. It is accordance with the conclusion from the COD and ICE data. This indicates that the synergistic effect of PC and EC oxidation is generated in the PEC process. Therefore, the intermediates can be removed efficiently and rapidly in the PEC process. According to the above analysis, we conclude that the possible degradation pathway of 2,4-D as follows (Scheme 2):

4. Conclusion

In summary, a facile liquid crystal soft template method constructed the 2D macroporous $\text{SnO}_2/\text{TiO}_2$ NTs catalyst. The prepared 2D macroporous $\text{SnO}_2/\text{TiO}_2$ NTs catalyst simultaneously possesses superior photocatalytic and electrocatalytic performance. It displayed excellent photoelectrocatalytic synergistic oxidation ability applying in the degradation of 2,4-D. The present concept of preparing 2D macroporous $\text{SnO}_2/\text{TiO}_2$ NTs will open a new avenue

to develop photoelectric functional materials with light transmittance and high surface area. This functional material has potential application in the environment, energy conversion/storage, and hydrolysis fields.

Acknowledgments

This work was supported jointly by the National Natural Science Foundation P.R. China (project no. 20877058), 863 Program (project no. 2008AA06Z329) from the Ministry of Science, and Nanometer Science Foundation of Shanghai (project no. 0852nm01200).

Appendix A. Supplementary data

Supplementary data associated with this article can be found, in the online version, at doi:10.1016/j.apcatb.2011.11.010.

References

- [1] X.Y. Yang, A. Wolcott, G.M. Wang, A. Sobo, B. Fitzmorris, F. Qian, J.Z. Zhang, Y. Li, *Nano Lett.* 9 (2009) 2331–2336.
- [2] B. Boye, E. Brillas, B. Marselli, P.A. Michaud, C. Comninellis, G. Farnia, G. Sandona, *Electrochim. Acta* 51 (2006) 2872–2880.
- [3] H. Lin, C.P. Huang, W. Li, C. Ni, S.I. Shah, Y.H. Tseng, *Appl. Catal. B: Environ.* 68 (2006) 1–11.
- [4] A. Wolcott, W.A. Smith, Y.P. Zhao, J.Z. Zhang, *Adv. Funct. Mater.* 19 (2009) 1849–1856.
- [5] X.Z. Li, H.L. Liu, P.T. Yue, Y.P. Sun, *Environ. Sci. Technol.* 34 (2000) 4401–4406.
- [6] X. Zhao, T.G. Xu, W.Q. Yao, C. Zhang, Y.F. Zhu, *Appl. Catal. B: Environ.* 72 (2007) 92–97.
- [7] M. Kitano, K. Funatsu, M. Matsuoaka, M. Ueshima, M. Anpo, *J. Phys. Chem. B* 110 (2006) 25266–25272.
- [8] D. Kibanova, J. Cervini-Silva, H. Destailats, *Environ. Sci. Technol.* 43 (2009) 1500–1506.
- [9] H. Tsuchiya, J.M. Macak, L. Taveira, E. Balaur, A. Ghicov, K. Sirotna, P. Schmuki, *Electrochim. Commun.* 7 (2005) 576–580.
- [10] Z.Y. Liu, X.T. Zhang, S. Nishimoto, T. Murakami, A. Fujishima, *Environ. Sci. Technol.* 42 (2008) 8547–8551.
- [11] X.H. Xia, Z.H. Jia, Y. Yu, Y. Liang, Z. Wang, L.L. Ma, *Carbon* 45 (2007) 717–721.
- [12] R. Ko'z, S. Stucki, B. Carcer, *J. Appl. Electrochem.* 21 (1991) 99–104.
- [13] B. Adams, M. Tian, A. Chen, *Electrochim. Acta* 54 (2009) 1491–1498.
- [14] H.L. Pang, J.P. Lu, J.H. Chen, C.T. Huang, B. Liu, X.H. Zhang, *Electrochim. Acta* 54 (2009) 2610–2615.
- [15] R. Sasikala, A. Shirole, V. Sudarsan, T. Sakuntala, C. Sudakar, R. Naik, S.R. Bhadraraj, *Int. J. Hydrogen Energy* 34 (2009) 3621–3630.
- [16] Z.Y. Liu, D.D.L. Sun, P. Guo, J.O. Leckie, *Nano Lett.* 7 (2007) 1081–1085.
- [17] G.H. Zhao, X. Cui, M.C. Liu, P.Q. Li, Y.G. Zhang, T.C. Cao, H.X. Li, Y.Z. Lei, L. Liu, D.M. Li, *Environ. Sci. Technol.* 43 (2009) 1480–1486.
- [18] P.Q. Li, G.H. Zhao, X. Cui, Y.G. Zhang, Y.T. Tang, *J. Phys. Chem. C* 113 (2009) 2375–2383.
- [19] X.H. Zhang, H. Liu, W.Z. Li, G.F. Cui, H.Y. Xu, K. Han, Q.P. Long, *Catal. Lett.* 125 (2008) 371–375.
- [20] J. Peller, O. Wiest, P.V. Kamat, *J. Phys. Chem. A* 108 (2004) 10925–10933.
- [21] A.M. LaChapelle, M.L. Ruygrok, M. Toomer, J.J. Oost, M.L. Monnie, J.A. Swenson, A.A. Compton, *Reprod. Toxicol.* 23 (2007) 20–31.
- [22] Q.Q. Wang, A.T. Lemley, *Environ. Sci. Technol.* 35 (2001) 4509–4514.
- [23] E. Brillas, J.C. Calpe, J. Casado, *Water Res.* 34 (2000) 2253–2262.
- [24] X. Cui, G.H. Zhao, Y.Z. Lei, H.X. Li, P.Q. Li, M.C. Liu, *Mater. Chem. Phys.* 113 (2009) 314–321.
- [25] M.H. Zhou, Q.Z. Dai, L.C. Lei, C. Ma, D.H. Wang, *Environ. Sci. Technol.* 39 (2005) 363–370.
- [26] S.U.M. Khan, M. Al-Shahry, W.B. Ingler, *Science* 297 (2002) 2243–2245.
- [27] S. Fierro, L. Ouattara, E.H. Calderon, E. Passas-Lagos, H. Baltruschat, C. Comninellis, *Electrochim. Acta* 54 (2009) 2053–2061.
- [28] P. Lhotak, S. Shinkai, *J. Phys. Org. Chem.* 10 (1997) 273–285.
- [29] D. Robert, *Catal. Today* 122 (2007) 20–26.
- [30] C. Borras, C. Berzoy, J. Mostany, J.C. Herrera, B.R. Scharifker, *Appl. Catal. B* 72 (2007) 98–104.
- [31] P. Liska, K.R. Thampi, M. Gratzel, D. Bremaud, D.H. Rudmann, M. Upadhyaya, A.N. Tiwari, *Appl. Phys. Lett.* 88 (2006) 203103.
- [32] D.B. Kuang, C. Klein, S. Ito, J.E. Moser, R. Humphry-Baker, N. Evans, F. Durrant, C. Graetzel, S.M. Zakeeruddin, M. Gratzel, *Adv. Mater.* 19 (2007) 1133.